D2.5 – Validation of cylinder geometry-based simulation of the closed loop geothermal system

Deliverable No.: D2.5

Deliverable lead: IFE

Authors: V. Leontidis, M. Wangen, N. Anand, F. Tosto

Dissemination level: PU

Submission date: 28.03.2024

Funded by the European Union. Views and opinions expressed are however those of the author(s) only and do not necessarily reflect those of the European Union or CINEA. Neither the European Union nor the granting authority can be held responsible for them.

PROJECT INFORMATION

PROJECT ACRONYM	HOCLOOP
Call ID	HORIZON- CL5-2021-D3-03-15
Project title	A circular by design environmentally friendly geothermal energy solution based on a horizontal closed loop - HOCLOOP
Grant Agreement No	101083558
Start of Project	01.10.2022
Project Duration	42 Months
Type of Action	HORIZON Research and Innovation Actions
Coordinator	IFE

DOCUMENT INFORMATION

Deliverable No.	D2.5
Work Package	WP2
Deliverable Lead	IFE
Deliverable Authors	V. Leontidis (IFPEN), M. Wangen (IFE), N. Anand (VITO), F. Tosto (VITO)
Issue	1/1
Due date	31.03.2023
Submission date	28.03.2024
Dissemination level[1]	PU
Nature[2]	R
Copyright	© 2023 Consortium

[1] Dissemination level: **PU** = Public, **SEN** = Sensitive, **R-UE/EU-R** = EU classified, **C-UE/EU-C** = EU classified, **S-UE/EU-S** – EU classified

[2] Nature of the deliverable: deliverable: **R** = Document, report; **DEM** – Demonstrator, pilot, prototype; **DEC** – Websites, patent, filings, videos etc; **DATA** – data sets, microdata, etc; **DMP** – Data Management Plan; **ETHICS**; **SECURITY**; **OTHER**

This project has received funding from the European Union's Horizon Europe research and innovation program under grant agreement No 101083558

DOCUMENT HISTORY

DATE	VERSION	MODIFIED BY	COMMENT
04.03.2023	0.1	V. Leontidis (IFPEN), M. Wangen (IFE), N. Anand (VITO), F. Tosto (VITO)	First draft for internal revision
11.03.2024	0.2	Mario Silva (IFE)	First internal revision
11.03.2024	0.3	Mario Silva (IFE)	Distributed for peer review
28.03.2024	0.4	Hung Pham (TUDa), Daniele Fiaschi (UNIFI)	Reviewer's comments
28.03.2024	1.0	Mario Silva (IFE)	Review addressed
28.03.2024	2.0	Mario Silva (IFE)	Final version

This project has received funding from the European Union's Horizon Europe research and innovation program under grant agreement No 101083558

TABLE OF CONTENT

PROJECT INFORMATION 2
DOCUMENT INFORMATION 2
DOCUMENT HISTORY 3
TABLE OF CONTENT 4
LIST OF TABLES 5
LIST OF FIGURES 5
LIST OF ABBREVATIONS 6
EXECUTIVE SUMMARY 7
1. Introduction 8
2. Sensitivity studies 9
2.1. GWellFM simulator 9
2.2. The simulator GTW 13
3. Optimization of concentric pipes 17
3.1. Baseline geometry 17
3.1.1. CFD Setup 17
3.1.2. Mesh Convergence Study 19
3.1.3. Analysis of CFD Results (Baseline geometry) 19
3.2. Design Optimization: Parametric Study 21
3.2.1. Methodology 21
3.2.2. Results 23
4. Conclusions 26
5. References 27

This project has received funding from the European Union's Horizon Europe research and innovation program under grant agreement No 101083558

LIST OF TABLES

Table 1. List of analytical and numerical tools. 8
Table 2. Inlet conditions, boundary conditions and geometric well characteristics. 9
Table 3. Impact of the grid size of the formation mesh close to the wellbore. 9
Table 4. Impact of the number of total cells of the formation mesh. 9
Table 5. Impact of initial time step. 10
Table 6. Impact of time increment step 10
Table 7. Impact of rocks domain size. 10
Table 8. Summary of GWellFM's results and set of tested numerical parameters. 13
Table 9. Key parameters and boundary for the baseline case. 18
Table 10. Setup of the CFD solver. 19
Table 11. Different test cases with ribbed fins 23

LIST OF FIGURES

Figure 1. Representation of the cross-section of the well completion with the different layers. 8
Figure 2. Impact of the grid size of the formation mesh close to the wellbore on fluid's outlet temperature. 11
Figure 3. Impact of the number of total cells of the formation mesh on fluid's outlet temperature. 11
Figure 4. Impact of initial time step on fluid's outlet temperature. 12
Figure 5. Impact of time increment step on fluid's outlet temperature. 12
Figure 6. Impact of the radius of the surrounding rocks domain on fluid's outlet temperature. 13
Figure 7. The three different radial resolutions used to test the simulator GTW. 14
Figure 8. The output temperature for the 9 different grid resolutions 14
Figure 9. The difference in output temperature between the 9 cases and the case with finest resolution. 15
Figure 10. The difference in output temperature between the analytical solution and the numerical solutions with different grid resolutions. 15
Figure 11. Computational flow domain and boundary conditions. 18
Figure 12. Computational grid used for the numerical simulations of the baseline geometry. 19
Figure 13. Nusselt number and friction factor coefficient values obtained from CFD simulations, and the correlations. 21
Figure 14. Baseline geometry with FFD-boxes. 22
Figure 15. Concentric pipe geometry with deformed FFD-boxes. 22
Figure 16. Concentric pipe geometry (left: inward ribbed fins, center: baseline, right: outward ribbed fins). 23
Figure 17. Variation of properties with bump height. Left: Nusselt Number; Right: Inlet, outlet, and logarithmic mean temperature. 23
Figure 18. Friction factor vs height of the ribbed fin. 24
Figure 19. Normalized pressure profile as a function of the streamwise coordinate for cases +1, 0 and -1 (bulk: streamline along the centerline of the annulus, wall: streamline close to the wall). 25

This project has received funding from the European Union's Horizon Europe research and innovation program under grant agreement No 101083558

LIST OF ABBREVATIONS

ACRONYM	DESCRIPTION
CFD	Computational Fluid Dynamics
GTW	Geo-Thermal-Well
GWellFM	Geothermal Well Flow Simulator
FFD	Free-Form Deformation
RANS	Reynolds Averaged Navier-Stokes
SST	Shear-Stress Turbulence

This project has received funding from the European Union's Horizon Europe research and innovation program under grant agreement No 101083558

EXECUTIVE SUMMARY

Scope of the deliverable

The objective of WP2 is to develop tools and models to predict the heat flow towards a closed-loop geothermal well and the associated temperature decrease of the surrounding rock. For this, local conditions are considered: rock properties, groundwater flow and the different layers of the walls of the well, such as casing and cement. Following the benchmarking of the available in-house codes in WP2.1 and WP2.2, as detailed in deliverables D2.1 [1] and D2.2 [2], the next goal was to validate the simulations in cylinder coordinates. The validation has considered the size of grid cells necessary to represent steep temperature gradients close to the well, the initial time step and the required radius of the surrounding rock to avoid boundary effects. The comparisons were based on available analytical solutions.

Besides, this deliverable also reports on the geometric optimization of the pipes. These results are an extension of the work reported in section D2.4 [3], where the effect of eccentricity was reported. Through this study, the shape of the outer pipes is morphed using a parametrization, and its affect on the performance parameters is assessed.

Main conclusions

The simulations of GWellFM shows that there is a critical radial grid size for which the numerical solution matches the analytical one. With further refinement of the grid, the gain in accuracy (when compared to the analytical solution) is very low but the computational cost increases. On the other hand, the time step has no practical impact on the results. The most important parameter is the radial size of the computational domain. If the domain is not sufficient large an impact of the boundary condition impose at the limit of the domain (null heat transfer) is observed on the results. At what distance from the wellbore and at which exact time the impact appears depends also on the overall simulation time.

The study of the grid resolution with the simulator GTW from IFE shows that increasing the grid resolution increases the precision of the numerical solution. Increasing the resolution in the radial direction beyond 50 cells (cell size 0.05 – 10 cm, depending on the case) made the numerical solution insignificantly better. The cells are assumed to form a geometrical series in the radial direction., where the first cell next to the well is just a few centimetres. As with GWellFM, enough rock must be included in the radial direction to avoid the cooling of the rock reaching the outer boundary of the mesh. As a rule of thumb, a discretization of 100 cells (cell size 0.05 – 10 cm, depending on the case) along the well gives a good numerical solution at a low computational cost.

In addition, the study on geometric optimization shows that the ribbed fins of different depths can affect the performance of the close-loop system. The results show that the ribbed fins of height ~2mm provide approximately 5.5% improvement in friction factor coefficient with a 3% impact on the Nusselt number. In order words, by incorporating a small bump, the pumping power can be reduced while reducing the overall heat transfer coefficient.

This project has received funding from the European Union's Horizon Europe research and innovation program under grant agreement No 101083558

1. Introduction

In the first deliverable of WP2 of the project [1], two in-house simulators (GWellFM from IFPEN and GTW from IFE) were benchmarked against analytical solutions for single injection wells [4] and closed-loops [5] (Table 1). These solutions considered uniform well configurations and homogeneous formation (constant rock properties). The Ramey solution was further expanded to consider heterogeneous formations or horizontal wells. It was shown that for a well-insulated inner tube in a coaxial configuration, the simple Ramey solution can predict quite accurate the temporal evolution of the fluid flowing in the casing. However, Sharma solution should be used for similar configurations.

Table 1. List of analytical and numerical tools.

Tool	Model	Type of simulations
Ramey [4]	Analytical	Injection well
Sharma [5]	Analytical	Coaxial L-shaped closed well
GWellFM (IFPEN)	Numerical	Any
GTW (IFE)	Numerical	Any

In addition, in deliverable D2.4 [3], simulations were performed for the actual configuration of the HOCLOOP solution (Figure 1) using the two above numerical tools. Several operational parameters were then modified to evaluate their impact on the performance of the closed loop.

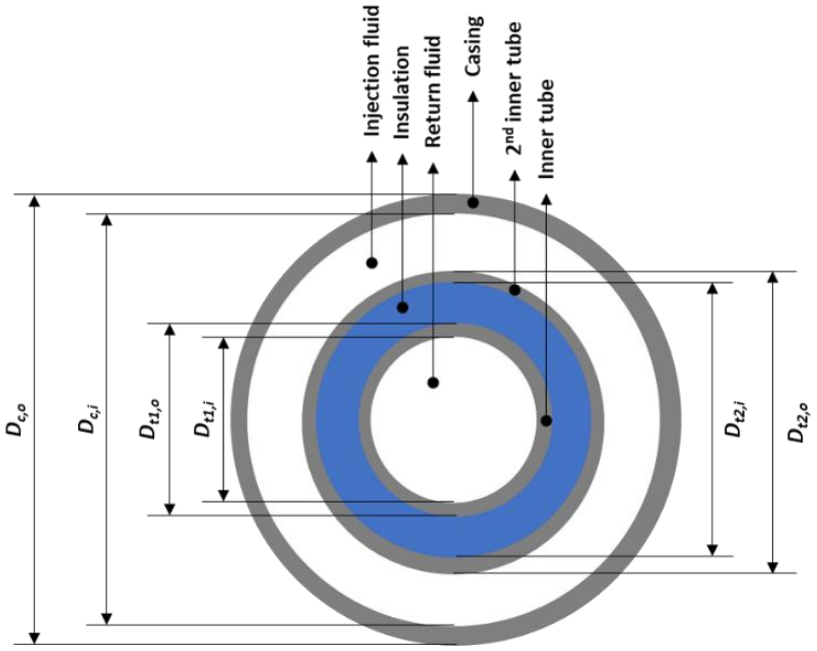

Figure 1. Representation of the cross-section of the well completion with the different layers.

This project has received funding from the European Union's Horizon Europe research and innovation program under grant agreement No 101083558

2. Sensitivity studies

2.1. GWellFM simulator

A realistic well configuration of the HOCLOOP solution was selected to study the impact of the numerical parameters (mesh, time step and domain size) on the results. The well consists of an external casing (c) and two inner tubes (t_1, t_2). Between the inner tubes, a layer of an insulation material is placed. The fluid is injected at the surface (with a constant flow rate, m, and temperature, T_{inj}) in the space between the casing and the second inner tube. Then, the fluid returns to the surface through the first inner tube. Here, and in contrast with the actual well configuration that was used in study of deliverable D2.4, the diameters of the vertical (depth, H) and the horizontal (length, L) wellbore are the same. Also, the properties (density, ρ, thermal conductivity, k, and heat capacity, C_p) of the rocks are constant in the whole domain (homogeneous hosting formation). The selection of these parameters was done to meet the constrains of the analytical solutions. The values of all parameters are detailed in Table 2.

Table 2. Inlet conditions, boundary conditions and geometric well characteristics.

Injection		Geometry		Insulation	Diameters				Rocks			
					Tubing		Casing					
m (kg/s)	T_{inj} (°C)	H (km)	L (m)	k (W/m/K)	$D_{t,i}$ (mm)	$D_{t,o}$ (mm)	$D_{c,i}$ (mm)	$D_{c,o}$ (mm)	g_T (°C/km)	k (W/m/K)	ρ (kg/m³)	C_p (J/kg/K)
5	30	4	5	0.01	85	122	101	140	194	172	30	3	2600	900

The below tables summarize the performed simulations. Sensitivity studies performed on 1) the grid size close to the wellbore (Table 3), 2) the total number of radial cells in the rock domain (Table 4), 3) the initial time step (Table 5), 4) the time step increasing factor (Table 6) and 5) the radial size of the domain (Table 7). The temporal evolution of fluid's outlet temperature is compared at all cases with the two analytical solutions of Table 1. For comparing the impact of the different numerical parameters on the performance of the code (computational demands) all simulation were executed on the same machine with the below specification:

- Intel Xeon 3.6 GHz 4 cores
- 64 GB DDR4 RAM memory

Table 3. Impact of the grid size of the formation mesh close to the wellbore.

Case	Domain			Time	
	Radius (m)	Number of radial cells	Size of 1st cell (cm)	Initial (s)	Step
1.1	50	50	10	43200	1.5
1.2	50	50	1	43200	1.5
1.3	50	50	0.1	43200	1.5
1.4	50	50	0.05	43200	1.5

Table 4. Impact of the number of total cells of the formation mesh.

Case	Domain			Time	
	Radius (m)	Number of radial cells	Size of 1st cell (cm)	Initial (s)	Step
2.1	50	15	0.1	43200	1.5
2.2	50	30	0.1	43200	1.5

This project has received funding from the European Union's Horizon Europe research and innovation program under grant agreement No 101083558

1.3	**50**	**50**	**0.1**	**43200**	**1.5**

Table 5. Impact of initial time step.

Case	Domain			Time	
	Radius (m)	Number of radial cells	Size of 1st cell (cm)	Initial (s)	Step
3.1	50	50	0.1	3600	1.5
3.2	50	50	0.1	7200	1.5
3.3	50	50	0.1	10800	1.5
3.4	50	50	0.1	21600	1.5
1.3	**50**	**50**	**0.1**	**43200**	**1.5**

Table 6. Impact of time increment step

Case	Domain			Time	
	Radius (m)	Number of radial cells	Size of 1st cell (cm)	Initial (s)	Step
4.1	50	50	0.1	43200	2
4.2	50	50	0.1	43200	1.2
1.3	**50**	**50**	**0.1**	**43200**	**1.5**

Table 7. Impact of rocks domain size.

Case	Domain			Time	
	Radius (m)	Number of radial cells	Size of 1st cell (cm)	Initial (s)	Step
5.1	5	30	0.1	43200	1.5
5.2	15	30	0.1	43200	1.5
5.3	30	30	0.1	43200	1.5
5.4	100	30	0.1	43200	1.5
2.2	**50**	**30**	**0.1**	**43200**	**1.5**

Figure 2 to Figure 6 present the evolution of fluid's outlet temperature in time for the different sensitivity studies, whereas Table 8 summarizes the computation time and the minimum and maximum difference between the numerical results and the analytical solution of Sharma for all cases. Sharma solution was chosen for comparison because it has been proven to be more accurate than the Ramey solution for this type of well configurations. However, the results of Ramey solution were included also in the figures.

Refining the cell grid closer to the wellbore lead to better results in comparison to Sharma's analytical solution (Figure 2). There is an optimal size (1 mm) below which the results remain the same, without also affecting the computational time. Refining the mesh in the formation domain by increasing the number of the grids but keeping constant the size of the grid close to the wellbore has not practical impact (Figure 3), while the computational demands are slightly higher.

This project has received funding from the European Union's Horizon Europe research and innovation program under grant agreement No 101083558

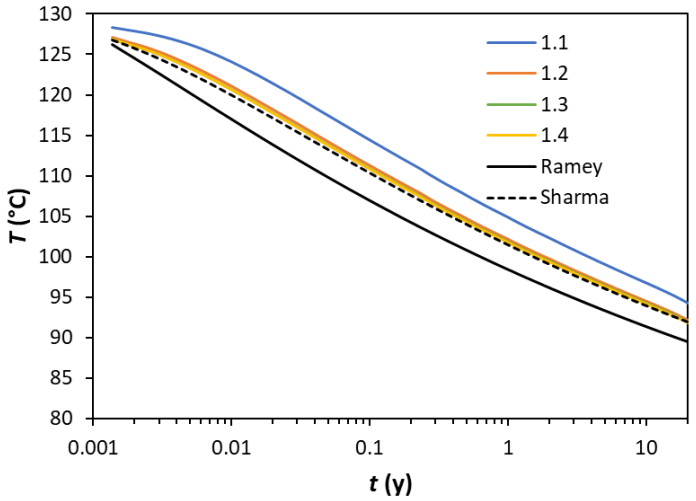

Figure 2. Impact of the grid size of the formation mesh close to the wellbore on fluid's outlet temperature.

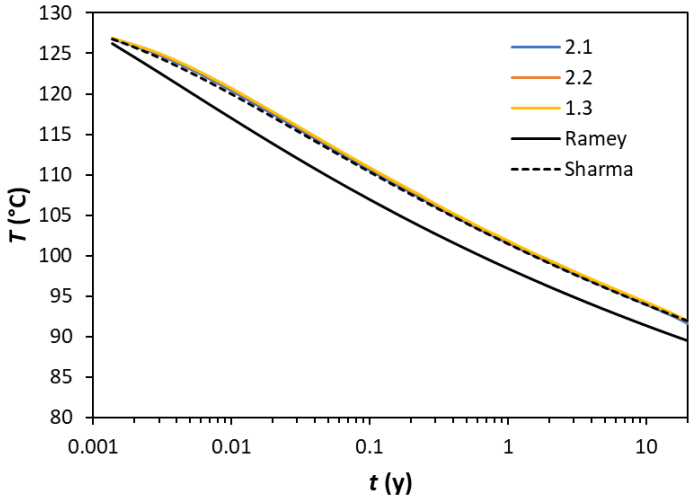

Figure 3. Impact of the number of total cells of the formation mesh on fluid's outlet temperature.

For smaller initial time steps, the deviation with the analytical solution increase at the early stages, while after few time steps are converging and giving the same results as before. The impact of the time step size is significant in the simulation time, as it increases considerable for smaller steps. For the smaller time step tested, the numerical tool couldn't converge for the specific numerical set-up, which could be attributed to the fact that flow in the wellbore has not reach the steady-state. The numerical tool assumes that the fluid and heat flow inside the wellbore is always (for every time step) at steady-state [1]. Modifying the increment step of the time step doesn't have a practical impact on the results (Figure 5) but only on the computational demands. The smaller the step increase is, the higher is the required time because more time steps are required.

This project has received funding from the European Union's Horizon Europe research and innovation program under grant agreement No 101083558

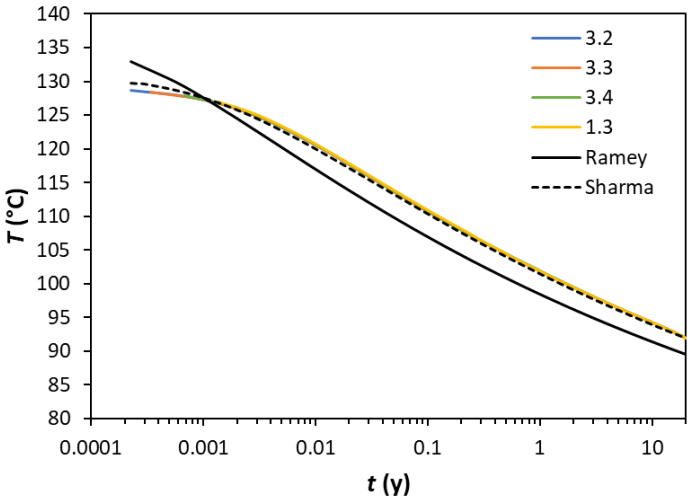

Figure 4. Impact of initial time step on fluid's outlet temperature.

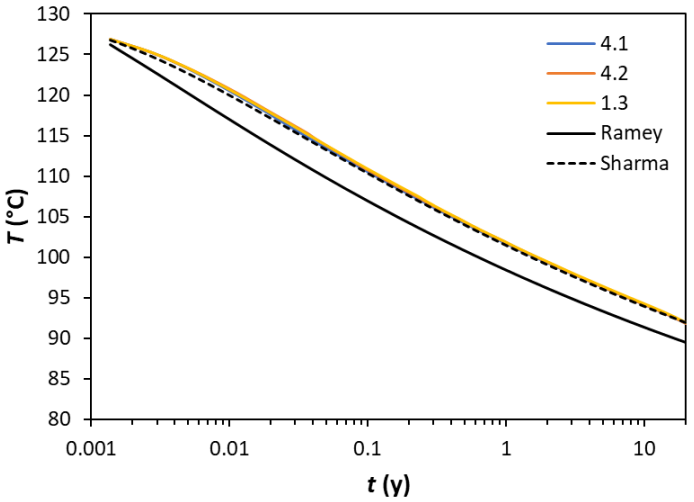

Figure 5. Impact of time increment step on fluid's outlet temperature.

The radius of the domain has a big impact on the results. The smaller the domain is, the more profound is the impact on the results (Figure 6). The boundary condition of null heat transfer in the limit of the domain affects the temperature of the fluid in the well. For each tested case, there is a specific time at which the results started to be affected by the boundary condition. Before this time all results are almost identical. For 20 years of operation a radius of 50 m seems to be sufficient.

This project has received funding from the European Union's Horizon Europe research and innovation program under grant agreement No 101083558

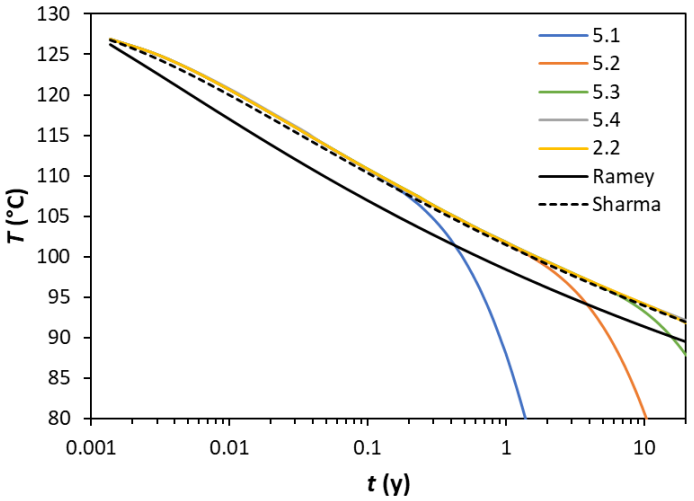

Figure 6. Impact of the radius of the surrounding rocks domain on fluid's outlet temperature.

Table 8. Summary of GWellFM's results and set of tested numerical parameters.

Case	Time (min)	δ (%) Min	δ (%) Max	Sensitivity parameter	Δr_1 (cm)	N	t_0 (h)	Δt	R (m)
1.1	145	1.186	3.681	Decrease size of 1st radial cell	**10**	50	12	1.5	50
1.2	127	0.204	0.914		**1**	50	12	1.5	50
1.3	124	0.000	0.580		**0.1**	50	12	1.5	50
1.4	124	0.006	0.560		**0.05**	50	12	1.5	50
2.1	95	0.002	0.379	Increase number of radial cells	0.1	**15**	12	1.5	50
2.2	106	0.006	0.550		0.1	**30**	12	1.5	50
3.1	-	-	-	Increase initial time step	0.1	**50**	1	1.5	50
3.2	152	0.000	0.801		0.1	50	**2**	1.5	50
3.3	144	0.000	0.757		0.1	50	**3**	1.5	50
3.4	124	0.000	0.529		0.1	50	**6**	1.5	50
4.1	229	0.001	0.491	Increase time step	0.1	50	12	**1.2**	50
4.2	109	0.000	0.661		0.1	50	12	**2**	50
5.1	102	0.100	67.612	Increase domain radius	0.1	30	12	1.5	**5**
5.2	117	0.063	30.615		0.1	30	12	1.5	**15**
5.3	119	0.006	4.529		0.1	30	12	1.5	**30**
5.4	101	0.000	0.653		0.1	30	12	1.5	**100**

2.2. The simulator GTW

The sensitivity of IFE's in-house simulator GTW for grid resolution was tested. The test cases were based on the reference case of WP 2.4. The reference case uses thermodynamic data for H_2O. We made two changes to the reference case of WP 2.4. The vertical and the horizontal wells were reduced from 4 km to 3 km. The reason was to ensure that the temperatures in the borehole were always less than 100 °C, thereby avoiding the possibility of two-phase flow.

GTW simulates a geothermal coaxial borehole heat exchanger assuming cylinder symmetry around the

This project has received funding from the European Union's Horizon Europe research and innovation program under grant agreement No 101083558

centre axis of the well. The numerical mesh becomes a 2-D grid where the radial x-axis is normal to the well and the y-axis follows the well. The well part of the grid is user-specified. In the radial direction, the 8 first cells are user input. These cells cover the inner tube, the insulation between the inner tube and the annulus, the annulus and three layers outside the annulus. The cells that cover the rock outside the third layer are automatically gridded with a geometric series that fills out the mesh to the maximum radius. In these cases, the maximum radius is 100 m.

Nine different resolutions were tested. The three radial resolutions 18, 48 and 108 were combined with the 3 different resolutions along the well. The two well segments were discretized with 30, 60 and 120 cells, which corresponds to cell lengths of 100 m, 50 m and 25 m, respectively. Figure 7 shows the 3 radial grid resolutions. Using 18 cells in the radial grid gives a very coarse discretization, where the largest cell has a radial extent of nearly half the maximum radius.

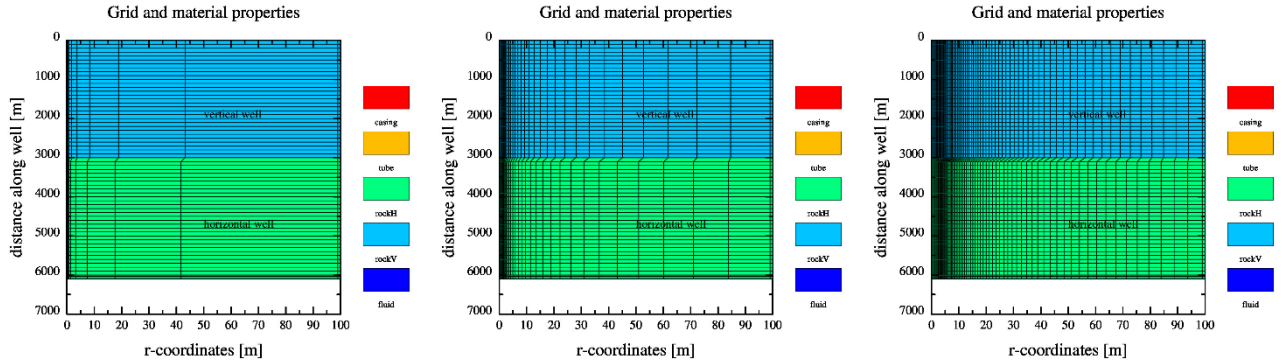

Figure 7. The three different radial resolutions used to test the simulator GTW.

Figure 8 shows the output temperature of the 9 simulations. The plot shows that even the coarsest grid gives an excellent match against the results of finer resolutions. To look more closely at the differences between the simulations, the difference between the output temperature for all cases was plotted against the output temperature of the case with the finest resolution.

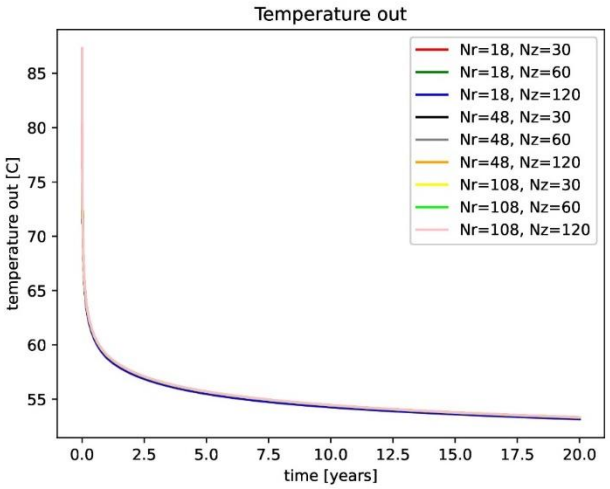

Figure 8. The output temperature for the 9 different grid resolutions

Figure 9 shows the difference in output temperature of the different cases. The case with the coarsest

This project has received funding from the European Union's Horizon Europe research and innovation program under grant agreement No 101083558

discretization in the radial direction (18 cells) has the largest difference against the case with the finest resolution. The plot shows that increasing the resolution increases the convergence against the case with the finest resolution. Since the cases with moderate resolution, such as the case in the middle with Nr = 48 and Nz = 60, are close to the case of fine resolution, there seems to be little to gain by using a very fine grid resolution.

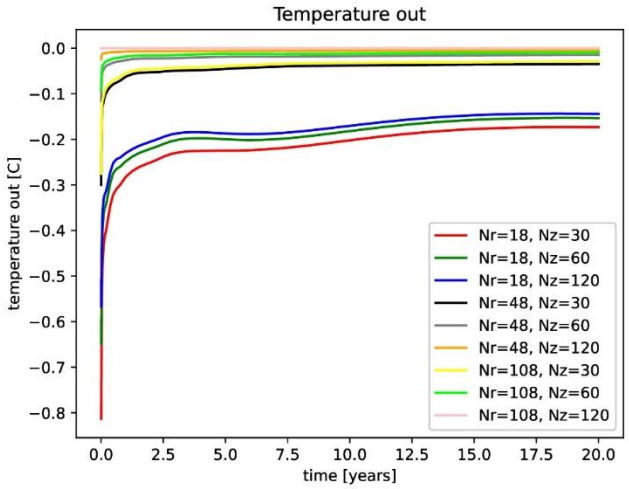

Figure 9. The difference in output temperature between the 9 cases and the case with finest resolution.

The same test series were performed against the analytical solution of Sharma [5]. The semi-analytical solution applies with a constant flow rate of an incompressible fluid. Furthermore, heat generation from friction is zero. The fluid parameters in the test cases are density = 998.5 kg/m^3, viscosity = 0.0011 Pa-s, compressibility = 0, expansibility = 0, heat capacity = 4196 J/kg-K and heat conductivity 0.58 W/m-K.

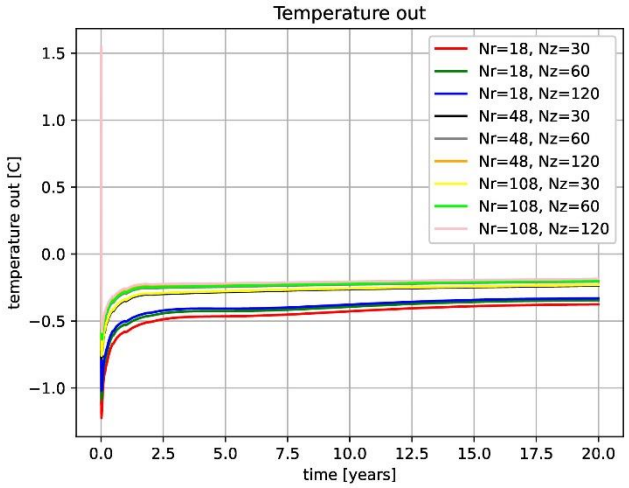

Figure 10. The difference in output temperature between the analytical solution and the numerical solutions with different grid resolutions.

Figure 10 shows the difference between the analytical output temperature and the 9 cases with different grid resolution. Increasing the grid resolution produces a numerical solution that is closer to the analytical solution. The coarsest grid gives an output temperature that is farthest away from the reference solution,

This project has received funding from the European Union's Horizon Europe research and innovation program under grant agreement No 101083558

and the finest grid gives the closest one. The difference is typically 0.2 °C for all cases, except the three cases with a coarse resolution in the radial direction. The remaining 0.2 °C difference could be linked to the thickness of the user-given layers for the casing and the cement in the well.

There is a spike in Figure 10 at the very beginning of the simulations. It is because of a weakness of the analytical solution for a short time. The solution is based on Ramey's approximation of the heat flow into a well. Ramey's approximation is inaccurate for times less than a week. The first step is 1 day, and the difference is 1.5 °C. After a few days, Ramey's approximation becomes accurate, and the difference drops to about 0.2 °C.

This project has received funding from the European Union's Horizon Europe research and innovation program under grant agreement No 101083558

3. Optimization of concentric pipes

The objective of this task is to obtain a concentric pipe geometry with improved heat-transfer and pressure-drop performance as compared to the baseline geometry. This is to be obtained by making modification to the surface of the outer pipe. Such modifications in the geometry can arguably lead to a decrease in the overall pressure drop, i.e., an improvement in the fluid dynamic performance, consequently requiring a smaller pump and less electricity consumption. In addition, such geometries could also potentially lead to configurations with high heat transfer coefficient leading to a higher overall heat extraction from the geothermal power plant.

A better heat transfer performance can arguably be obtained by increasing the overall heat transfer area. One of the ways to obtain this is by introducing annular bumps/fins on the outer pipe of the system which is in direct contact with the rocks in the proposed geothermal plant.

To study such pipe geometries, a concentric pipe configuration used in the project will be selected and evaluated at its baseline configuration. The selected configuration will be then optimized using VITO's inhouse design optimization framework. The optimization software consists of a volume mesh deforming algorithm and a CFD solver. The flow was simulated using the Reynolds Averaged Navier Stokes (RANS) equations, and the turbulence will be modelled using the two equation Shear-Stress Turbulence (SST) model [6, 7]. In addition, to reduce the computation cost of numerical simulations, a streamwise periodic flow assumption will be made for the pipe channels [8]. Thanks to the use of this streamwise periodic flow model, only a small section of the pipe can be simulated to predict the performance of a long pipe. The thermos-physical quantities will be assumed to be constant in the flow domain.

This research focuses on the HOCLOOP configuration as reported in D2.4 and this configuration will be used for the case study. In addition, to limit the number of simulations, the performance will be evaluated at the centre of the horizontal pipe at a steady-state condition of 10 years as reported for case f in D2.4.

3.1. Baseline geometry

The test case used in this research is the HOCLOOP's concentric pipe configuration, as reported in D2.4. To perform simulations in the context of current research only on the fluid flowing through the outer pipe is required. Table 9 lists the main geometrical parameters and the boundary conditions used to perform CFD analysis.

3.1.1. CFD Setup

A CFD simulation of the annular passage of the baseline geometry has been performed using the open-source CFD-solver SU2 [6]. The flow in the passage has been simulated using the incompressible Reynolds Averaged Navier-Stokes (RANS) equations. The turbulence has been modelled using the two equation Shear-Stress Turbulence model [7]. The steady state solution has been obtained by using a fixed-point iterator with a pseudo time stepping approach. To reduce the computation cost, streamwise periodic flow equation were solved. The working fluid is liquid water. The thermo-physical properties of the fluid were assumed to be constant in the flow domain.

This project has received funding from the European Union's Horizon Europe research and innovation program under grant agreement No 101083558

Table 9. Key parameters and boundary for the baseline case.

No.	Parameter	Values	Units	Data source
1	Diameter outer (Casing inner)	0.175	m	(Table1, D2.4)
2	Diameter inner (Insulation outer)	0.140	m	
3	Heat flux*	266.5216 @10Yrs	W/m^2	Data file from Edgar Hernandez Acevedo (22/06/23)
4	Temperature in Horizontal section	57.7 @10Yrs	°C	
5	Mass flow rate	5	kg/sec	(Table10, D2.1)
6	Viscosity	0.0011	Pa·s	(Table 8, D2.1)
7	Density	998.55	kg/m^3	(Table 8, D2.1)
8	Pr (lam,turb)	7.11/1.9	-	CoolProp/Kays(1994)
9	Re_{Dh}	18368.28	-	

To simulate the flow in an annulus, a constant mass flow rate was specified according to the value in Table 9, whereas iterations compute the pressure drop per unit length. To obtain a condition like that in the actual operation conditions, the outer surface of the outer pipe is specified with constant heat flux values as specified in Table 9. The inner wall of the annulus is supposed to be adiabatic, i.e., the local heat transfer is 0 W/m^2.

Figure 11 shows the computational flow domain with the specified boundary conditions. An overview of the simulation setup is reported in Table 10. Only convective heat transfer phenomena are investigated the heat conduction through the pipe walls is neglected.

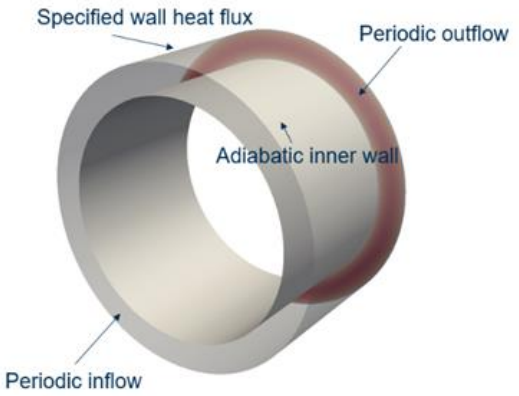

Figure 11. Computational flow domain and boundary conditions.

This project has received funding from the European Union's Horizon Europe research and innovation program under grant agreement No 101083558

Table 10. Setup of the CFD solver.

Options	Selections
Solver	Incompressible
Eqs.	RANS+SWP
Turb.	SST-m2003v
Thermophysical Properties	Constant density
Avg. y+	5
Kind SWP	Mass flow
Advection scheme	2nd order JST
# mesh elements	1,06 million

3.1.2. Mesh Convergence Study

The mesh convergence study is an essential step in CFD-based numerical analysis to estimate the discretization error that might exist in the case under study. The mesh used in this study consist of quadrilateral elements in the proximity of the wall, and unstructured tetrahedral elements in the bulk flow domain. To save on the computational resources, the mesh density parameters as reported in D2.2 for case f will be used in this study. By inheriting the same mesh generation setup used for D2.2 case f, the results presented in the following can also be reasonably deemed grid independent. For completeness, the mesh used for the study here onwards is reported in Figure 12. The total number of elements is ~1.06 million.

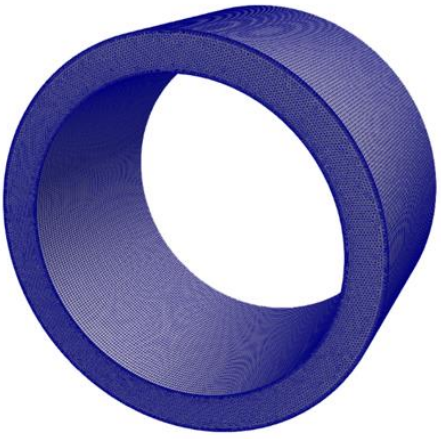

Figure 12. Computational grid used for the numerical simulations of the baseline geometry.

3.1.3. Analysis of CFD Results (Baseline geometry)

The heat transfer performance and the fluid-dynamic loss of the device was assessed by inspecting the values of the Nusselt number and the friction factor from the results of the CFD computations, respectively.

The Nusselt number is defined as:

$$Nu_{CFD} = \frac{hD_h}{k} \quad (1)$$

here h is the overall heat transfer coefficient, $D_h = D_{out} - D_{in}$ is the hydraulic diameter of the annular pipe, and k is the thermal conductivity of water, whereas the friction coefficient is defined as:

This project has received funding from the European Union's Horizon Europe research and innovation program under grant agreement No 101083558

$$f_{CFD} = \frac{2\Delta P D_h}{\rho V^2 l} \tag{2}$$

where ρ and V are the fluid density and the flow speed, respectively, and l is the axial length of the pipe section.

The values of these two non-dimensional parameters obtained from the CFD results have been compared with those obtained from correlations either available in the literature or provided in deliverables D2.1 (Eqs. 4-5, for Nusselt number) [1] and D2.2 (Eqs. 8-10, for the friction factor) [2]. The correlations used for the Nusselt number are:

1. Dittus-Boelter, valid only for full circular pipes:

$$Nu = 0.023 Re^{0.8} Pr^{0.4} \tag{3}$$

where $Re = \frac{\rho V D_h}{\mu}$ is the flow Reynolds number and $Pr = \frac{\mu}{c_p k}$ is the fluid Prandtl number, being μ and c_p the dynamic viscosity and the specific heat capacity of the working fluid.

2. VDI Heat Atlas [9]

$$Nu = \frac{(f/8) RePr}{k_1 + 12.7\sqrt{f/8}\,(Pr^{2/8} - 1)} \left| 1 + \left(\frac{D_h}{l}\right)^{\frac{2}{3}} \right| F_{ann} \tag{4}$$

where f is the friction factor computed using the model reported in [10], and:

$$k_1 = 1.07 + \frac{900}{Re} - \frac{0.63}{1 + 10\,Pr} \tag{5}$$

The correlations used for the friction factor are:

1. Correlation from D2.2 [2]

$$f = 8\left[\left(\frac{8}{Re}\right)^{12} + \left(\frac{1}{\theta_1 + \theta_2}\right)^{\frac{3}{2}}\right]^{1/12} \tag{6}$$

where:

$$\theta_1 = \left[2.457 \ln\left(\frac{1}{\left(\frac{7}{Re}\right)^{\frac{9}{10}} + \frac{0.27\epsilon}{D_h}}\right)\right]^{16}$$
$$\theta_2 = \left(\frac{37530}{Re}\right)^{16} \tag{7}$$

2. Dickinson (2017) [10]

$$f = (1.8 \log_{10} Re^* - 1.5)^{-2} \tag{8}$$

where:

$$Re^* = Re_{D_h} \frac{(1 + a^2)\ln a + (1 - a^2)}{(1 - a^2)\ln a}$$
$$a = \left(\frac{D_{in}}{D_{out}}\right) \tag{9}$$

This project has received funding from the European Union's Horizon Europe research and innovation program under grant agreement No 101083558

Figure 13 reports the values of both the Nusselt number, and the friction factor obtained from the CFD and from the empirical models listed above. It can be observed that the value of the friction factor obtained using the correlation provided in D2.2 is 16.57% larger than that obtained from the CFD, whereas the estimation obtained using the Dickinson model is in line with CFD (-2.9%). Regarding the Nusselt number, both correlation overpredict its value with respect to the CFD results: in particular, the values obtained using the VDI Heat Atlas [9] and the Dittus-Boelter correlations exceed the CFD one by 47.07% and 11.08%, respectively.

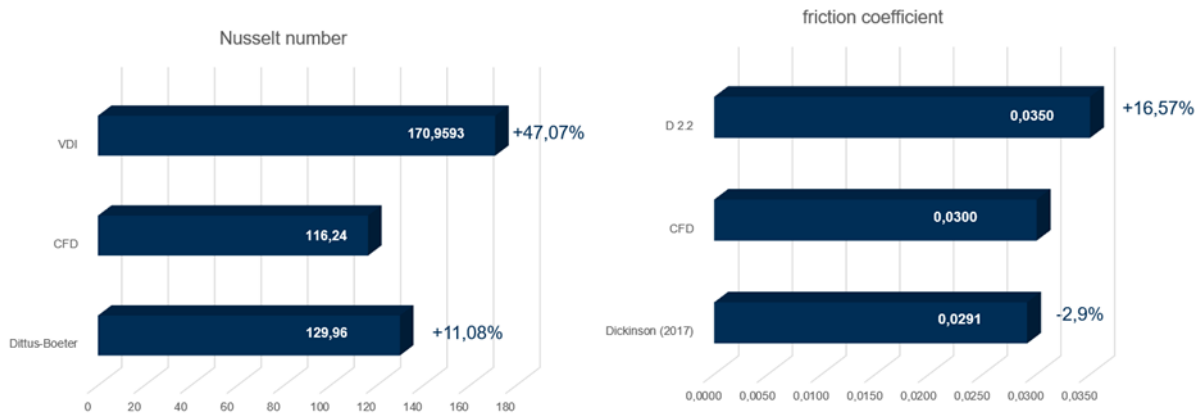

Figure 13. Nusselt number and friction factor coefficient values obtained from CFD simulations, and the correlations.

Apart from the correlation reported in [10], the values of both Nu and f obtained using the remaining empirical models largely deviate from those obtained from the CFD simulation. However, it should be noted that the Dittus-Boelter correlation for the Nusselt number is not valid for annular pipes, and that the correlation presented in D 2.2 for the friction factor was also not matching the CFD estimations conducted for case f, D2.4. The accuracy of this latter correlation is thus debatable.

3.2. Design Optimization: Parametric Study

To enhance the thermal performance of the concentric pipe configuration, a parametric study was performed. Different fin structures were generated and simulated using the open-source CFD suite SU2 [6]. The results from the simulation were then analysed to assess the thermo-hydraulic performance of the device.

3.2.1. Methodology

The parametric study has been conducted resorting to the surface mesh deformer (SU2_DEF) and the CFD solver (SU2_CFD) embedded in the SU2 suite. A free-form deformation (FFD) boxes approach [11] was used to deform the surface of the outer pipe. This simple method allows for an efficient parameterization of surfaces of arbitrary shapes. In the current study, a cylindrical FFD-boxes configuration was used to parametrize the outer wall of the concentric pipe (Figure 14). The FFD-boxes mesh consists of 2 points along the radial direction, 25 along the tangential one and 19 along the streamwise one, leading to a total of 950 design variables.

To have fins on the surface of the outer pipe, the design variables on the surface of the outer pipe were translated in the radial direction to obtain the deformed surface (Figure 15). Although a variety of fin configurations is possible using this method, the scope has been kept limited to practical designs. More specifically, such design has been kept limited to pipe geometries with rib like fins on the outer surface of

This project has received funding from the European Union's Horizon Europe research and innovation program under grant agreement No 101083558

the concentric pipes.

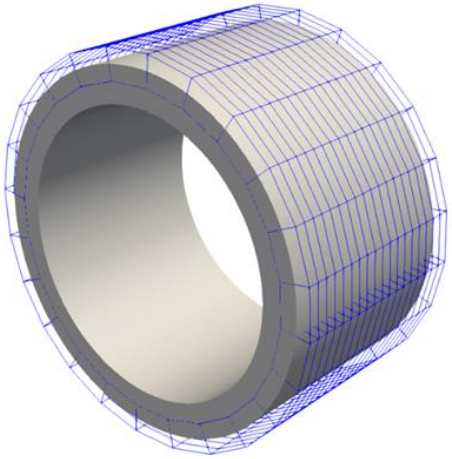

Figure 14. Baseline geometry with FFD-boxes.

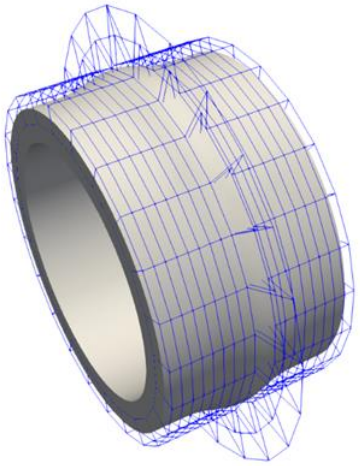

Figure 15. Concentric pipe geometry with deformed FFD-boxes.

The ribbed fins were generated on the outer wall surface according to two configurations: outward and inward fins (Figure 16). In addition, to study the influence of size of fin on the performance of the pipe, the fin height was varied for a range of values, as represented in Table 11. In the following, the individual case will be referred according to the nomenclature presented in the first column of Table 11. The baseline case will be referred to as 0 in the following.

This project has received funding from the European Union's Horizon Europe research and innovation program under grant agreement No 101083558

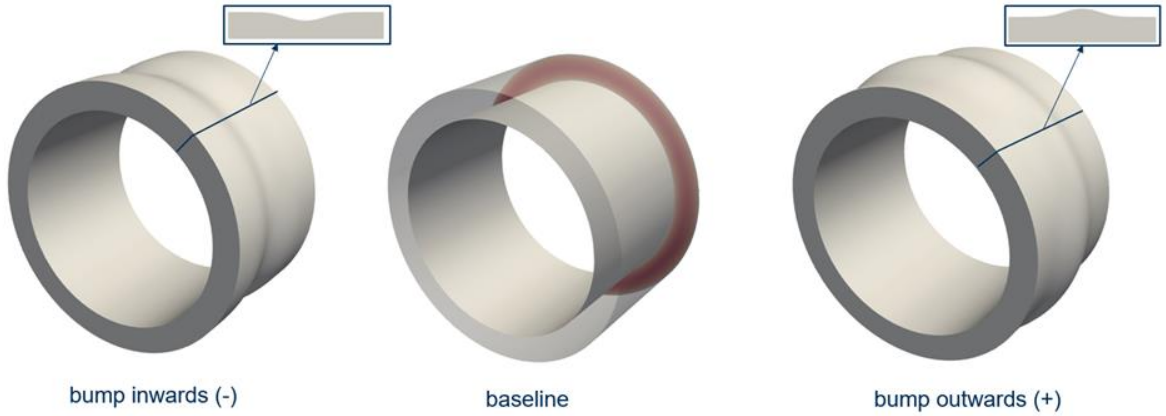

Figure 16. Concentric pipe geometry (left: inward ribbed fins, center: baseline, right: outward ribbed fins).

Table 11. Different test cases with ribbed fins

Test case	Bump height Δr [mm]
-3	- 5,57
-2	- 3,71
-1	- 1,86
+1	+ 1,86
+2	+ 3,71
+3	+ 5,57

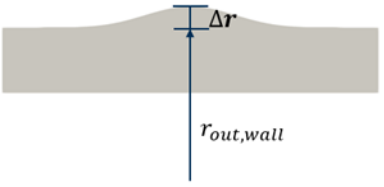

3.2.2. Results

Figure 17u(left) shows the variation of the Nusselt number as a function of the height of the ribbed fin, Δr. Although the heat transfer area increases with the height of the bump, a lower value of the Nusselt number and, consequently, of the heat transfer coefficient is recorded for the +1 case, which presents an outward fin. The relative increase on the Nusselt number with respect to the baseline case is 3.12%. Opposite trends are observed instead on Figure 17(right), the maximum wall and logarithmic temperatures are found for the +1 case.

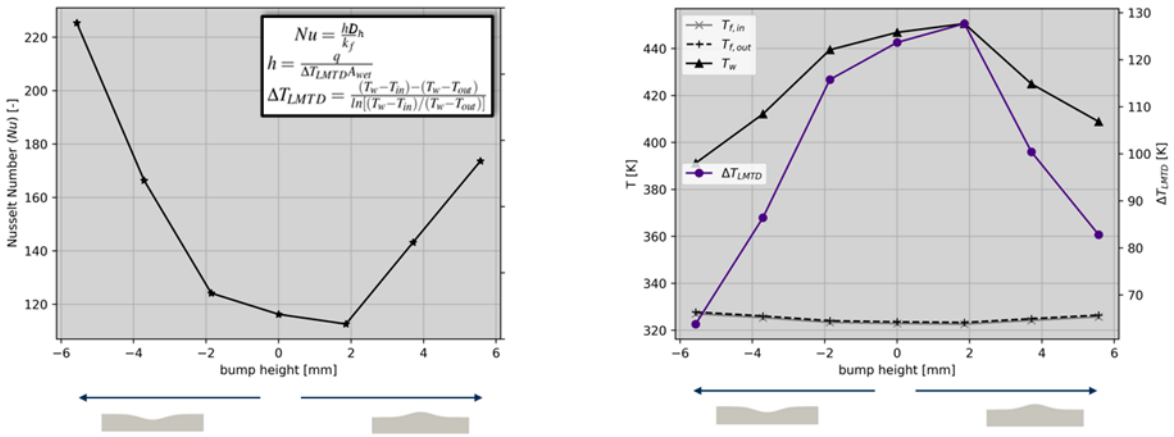

Figure 17. Variation of properties with bump height. Left: Nusselt Number; Right: Inlet, outlet, and logarithmic mean temperature.

This project has received funding from the European Union's Horizon Europe research and innovation program under grant agreement No 101083558

Adding a bump of $\Delta r \approx 2$ mm arguably leads to a decrease on the heat transfer capacity of the piping system with respect to the baseline design. Conversely, increasing the Δr value or opting for inwards ribbed fins leads to an increase on the Nusselt number and a better heat transfer performance compared to the baseline.

Figure 18 shows the variation of the friction factor as a function of the height of the ribbed fin. Also, for this parameter, the minimum value is recorded for the +1 case. Although having a detrimental effect on the heat transfer performance, the outwards 2 mm fin leads to a better fluid dynamic performance of the pipe, reducing the overall pressure drop of 5.48% with respect to the baseline geometry.

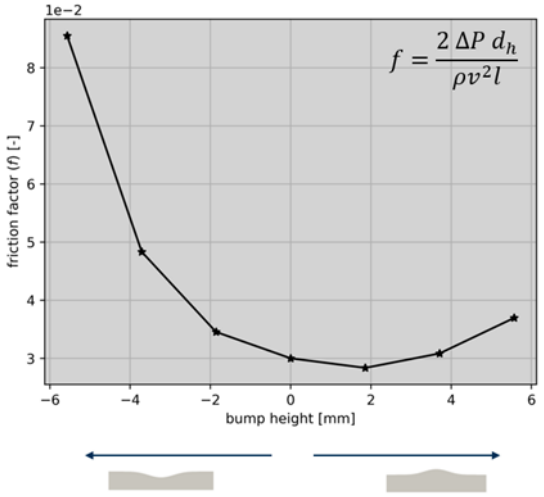

Figure 18. Friction factor vs height of the ribbed fin.

To understand the physics behind this phenomenon, the normalized pressure trends along the centreline of the annulus and in the proximity of the outer wall are plotted as a function of the streamwise coordinate. Trends for the +1, 0, and -1 cases are plotted. Each pressure value is normalized by the inlet pressure.

Compared to both the baseline and the -1 cases, the +1 case exhibits a more efficient pressure recovery in the aft part of the pipe section. This is arguably due to a beneficial effect of the local pressure gradient arising in the proximity of the fin on the overall dissipation due to friction. The local pressure near the wall is larger than the one measured in the baseline 0 case, and the dissipative phenomena occurring at the wall are therefore characterized by a lower local velocity. Being the dissipation proportional to the cube of the velocity, a lower friction factor coefficient is thus calculated for this finned geometry. If the height of the fin is low, this effect prevails over the detrimental one produced by the increase of the wetted area with respect to the baseline. By increasing the Δr, the contribution to the dissipation due to the increase in wetted area prevails, leading to an increase on the overall friction factor and a worse fluid dynamic performance, as observed for the +2 and +3 cases in Figure 19.

This project has received funding from the European Union's Horizon Europe research and innovation program under grant agreement No 101083558

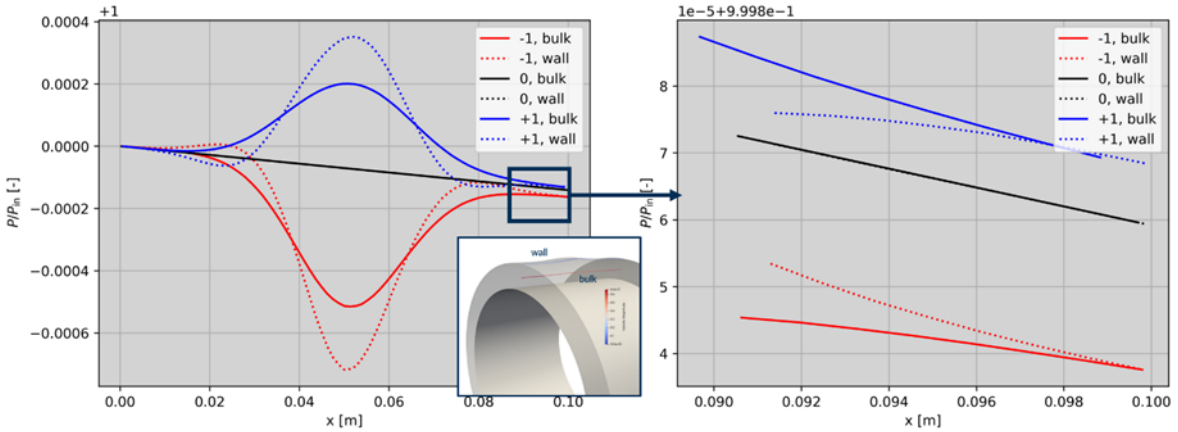

Figure 19. Normalized pressure profile as a function of the streamwise coordinate for cases +1, 0 and -1 (bulk: streamline along the centerline of the annulus, wall: streamline close to the wall).

This project has received funding from the European Union's Horizon Europe research and innovation program under grant agreement No 101083558

4. Conclusions

The simulations of GWellFM showed that there is a critical radial grid size for which the numerical solution matched the analytical one. Refining more the gain in accuracy is very but the computational cost increase. On the other hand, the time step had no practical impact on the results. The most important parameter was the overall radial size of the domain. If the domain is not sufficiently large, an impact of the boundary condition at the limit of the domain (null heat transfer) will be observed on the results. At what distance from the wellbore and at which exact time the impact will appear depends also on the overall simulation time.

The study of the grid resolution with the simulator GTW from IFE shows that increasing the grid resolution increases the precision of the numerical solution. A minimum resolution is needed in both the radial direction and along the well to ensure a good numerical solution. Increasing the resolution in the radial direction beyond 50 cells made the numerical solution insignificantly better. The cells are assumed to form a geometrical series in the radial direction, where the first cell next to the well is just a few centimetres. This is necessary to represent steep thermal gradients near the well. As with GWellFM, enough rock must be included in the radial direction to avoid the cooling of the rock reaching the outer boundary of the mesh. As a rule of thumb, a discretization of 100 cells along the well gives a good numerical solution at a low computational cost.

A CFD-based parametric study on the geometry of the outer wall of the supply pipe of the HOCLOOP system has been performed. The conclusions of the study are summarized in the following.

With regards to the baseline geometry:

- the Nusselt number value obtained with CFD simulation does not accurately correlate with both the Dittus-Boelter correlation (+11.08% on Nu) and the VDI correlation (+47.07% on Nu). However, the first correlation is only valid for full circular pipes, and the accuracy for annular pipes such as the configuration here investigated is debatable.
- the friction factor value obtained with CFD simulation accurately correlate with Dickinson model (-2.9% on f), while it does not correlate with correlation provided in D 2.2 (+16.57% on f).

The results of the parametric study on the geometry of the outer wall highlighted that adding an external annular bump of $\Delta r \sim 2$ mm on the outer wall leads to

- a decrease on the overall heat transfer coefficient of $\sim 3\%$;
- a decrease on the friction factor of $\sim 5.5\%$.

In summary, the authors recommend considering the modification of the geometry of the outer pipe here proposed if a lower pumping pressure at the supply side is desired.

This project has received funding from the European Union's Horizon Europe research and innovation program under grant agreement No 101083558

5. References

[1] E. Acevedo, V. Leontidis, M. Wangen and V. Harcouët-Menou, "Benchmark cases D2.1," HOCLOOP Project 101083558, 2023.

[2] V. Leontidis, M. Wangen, P. Ungar and D. Fiaschi, "Flow pipe model for fluid circulation D2.2," HOCLOOP Project 101083558, 2023.

[3] V. Leontidis, N. Anand and M. Wangen, "Deliverable D2.4: Optimized design for the closed loop geothermal system," 2023.

[4] H. Ramey Jr., "Wellbore heat transmission," *Journal of Petroleum Technology,* vol. 14, pp. 427-435, 1962.

[5] P. Sharma, A. Al Saedi and C. Kabir, "Geothermal energy extraction with wellbore heat exchanger: Analytical model and parameter evaluation to optimize heat recovery," *Renewable Energy,* vol. 166, pp. 1-8, 2020.

[6] T. A. Albring, M. Sagebaum and N. R. Gauger, "Efficient Aerodynamics design using the discrete adjoint method in SU2," in *17th AIAA/ISSMO Multidiscusplinary Analysis and Optimization Conference*, Washington DC, USA, 2016.

[7] F. R. Menter, "Two-Equation Eddy-Viscosity Turbulence Models for Engineering Applications," *AIAA Journal,* vol. 32, no. 8, pp. 1598-1605, 1994.

[8] S. Patankar, C. Liu and E. M. Sparrow, "Fully developed flow and hear transfer in ducts having streamwise-periodic variations of cross-sectional area.," *Journal of Heat Transfer,* vol. 99, pp. 180-187, 1977.

[9] M. Kind, D. Steiner, J. M. Chawla, J.-J. Schröder, Y. Saito, H. Auracher, O. Herbst and A. Katsaounis, "VDI Heat Atlas," *Springer,* 2010.

[10] D. D. Ndenguma, J. Dirker and J. P. Meyer, "Heat transfer and pressure drop in annuli with approximately uniform internal wall temperatures in the transitional flow regime.," *International journal of heat and mass transfer,* vol. 111, pp. 429-441, 2017.

[11] N. Anand, S. Vitale, M. Pini and P. Colonna, "Assessment of FFD adn CAD-based shape parametrization methods for adjoint-based turbomachinery shape optimization," in *GPPS Conference*, Montreal, 2018.

This project has received funding from the European Union's Horizon Europe research and innovation program under grant agreement No 101083558